Evolution of Microstructure and Texture in Ferritic FeSi Steels at Final Annealing – Role of Strain Induced Boundary Migration and Secondary Recrystallization

A. Franke, Juergen Schneider, Brigitte Bacroix

Proc. 9. International Conf. Magnetism and Metallurgy WMM20, November Rome, Italy (2020) p.349, ISBN 978-88-900033-1-8

Evolution of Microstructure and Texture in Ferritic FeSi Steels at Final Annealing – Role of Strain Induced Boundary Migration and Secondary Recrystallization

Franke A.[1], Schneider J.[1], Bacroix B.[2]
[1] Stahlzentrum Freiberg e.V., Leipziger Straße 34, 09599 Freiberg, Germany;
[2] LSPM – CNRS, UPR3407, Université Paris 13, 99, Av. J.B. Clément, 93430 Villetaneuse, France.

1 Introduction

The fabrication of non oriented electrical steels (NGO) with the desired thicknesses demands a large deformation rate at cold rolling. The final annealing has to be realized in a way that large grain sizes are obtained. This is finally reached by grain growth after recrystallization. A large grain size is necessary to get low magnetic specific losses. Furthermore, a high intensity of preferable magnetic texture components is desired to obtain a good magnetizing behavior. To realize a large grain size makes a big difference to the desired grain structure for steels. In addition, γ- fibre texture is not the desired texture for non oriented electrical steels.In this paper, we will analyze in detail the recrystallization behaviour followed by grain enlargement of ferritic FeSi 2.4 steels at final annealing. Thereby the complex heterogeneous deformation structure across the thickness after cold rolling has to be regarded. For the analysis we used the OIM, ODF the image quality (IQ) as well as the distribution function for the misorientation obtained from EBSD-measurements. The appearance of the different processes: recovery, recrystallization (nucleation and growth of nuclei; strain induced boundary motion), grain growth after the primary recrystallization: (continuous and /or discontinuous grain growth) are discussed.

2 Non-Oriented Electrical Steel

2.1 Microstructure of the Cold Rolled Material and Characteristic of the Strain Heterogeneities

Due to the variation of the parameters at final hot rolling one gets a variety of images for the microstructure after hot rolling. This results finally in quite different

microstruture and texture after cold rolling [1 - 4]. The OIM in Figure 1 presents typical features of the deformation structure after hot rolling of different fabricated hot band. The OIM indicate the presence of elongated bands oriented mainly in the rolling direction with γ- fibre texture (<111>parallel NR) and bands with mainly cube fibre texture (<001>parallel ND) These bands are distributed more or less over the thickness. Thereby the portion of the area with γ- fibre texture seems to be larger for the samples 2 and 7. The bands with with γ- fibre texture (<111>parallel NR) show a more or less high value of the image quality (IQ) at EBSD investigations. A band with cube fibre texture has high values of IQ. A high intensity of shear bands is visible especially in the areas with γ- fiber texture (<111>parallel NR) for samples 2 and 7. The regions with shear banding exhibit a low image quality (increasing lattice distortion). Zones with shear banding across the thickness are also very clear visible in the optical micrographs for these samples [1 -4]. With respect to an analysis of the evolution of microstructure and texture at annealing, it is interesting to note that substructures with high intensity of zones with shear banding have been also obtained in the case of using the strip-casting route after cold rolling [5 - 7].

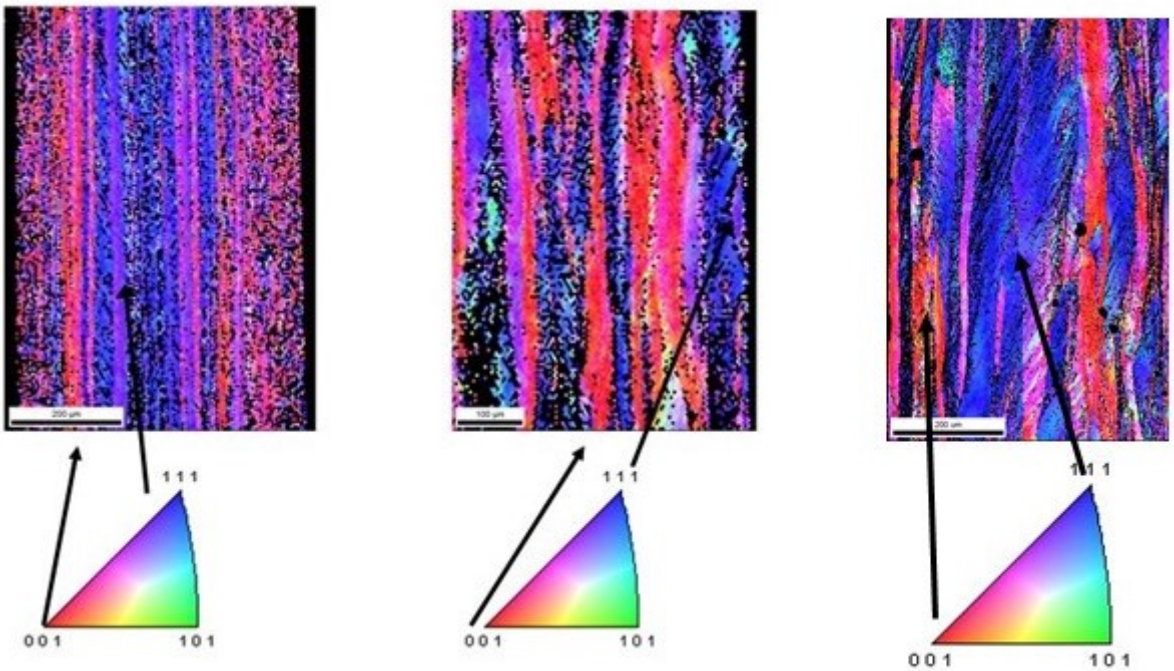

Sample 1 Sample 2 Sample 7

Fig. 1: OIM of sample 1, 2 and 7 after cold rolling

As shown in Figure 2, the image quality plus the rotation angle map (misorientation) is quite different for sample 1 and 2. The higher intensity of small angles for sample 2 may indicate a much stronger formation of sub grains due to the process of recovery compared to sample 1. Recovery comprises cancellation and rearrangement of

dislocations, which leads to the formation of sub grain structures with low angle boundaries [8, 9]. The deformation structure after cold rolling with large deformation is rather complex and spatial inhomogeneous, characterized by the fact that we have beside uniform stress is some areas also strain partitioning and strain location [10]. The complex locally rather inhomogeneous deformation structure after cold rolling reflects also in different texture. For sample 2 areas of bands with exhibit mainly a cube fibre texture one finds areas, where a strong rotated cube texture and α –fibre is observed.[3, 4]. Even more complex figures for texture after cold rolling are found especially between the bands oriented mainly in the rolling direction with γ- fibre texture (<111>parallel NR) and bands with cube fibre texture (<001>parallel ND), see Figure 3. One observes even small areas with some shear banding , where already very small grains appear between the shear lines. The texture nearby the shear line shows γ - fibre texture. The small grains exhibit cube fibre texture and α^* - texture, see Figure 4. These observed features for the microstructure of the cold rolled material, which is a consequence of the strong deformation rate at cold rolling,, will affect remarkable the ongoing processes at final annealing.

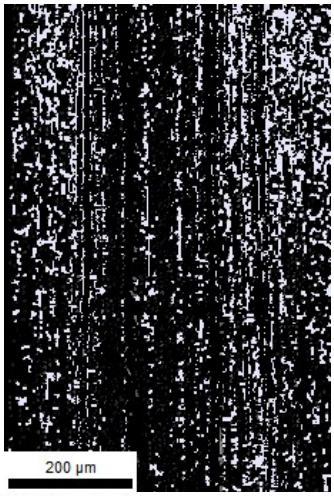

Boundaries: Rotation Angle

	Min	Max	Fraction	Number	Length
	15°	180°	0.488	33654	9.72 cm
	2°	15°	0.512	35264	10.18 cm

Boundaries: Rotation Angle

	Min	Max	Fraction	Number	Length
	15°	180°	0.216	9993	2.88 cm
	2°	15°	0.784	36271	10.47 cm

Fig. 2: Image quality plus the rotation angle map (misorientation) of sample 1 (left) and sample 2 (right) after cold deformation.

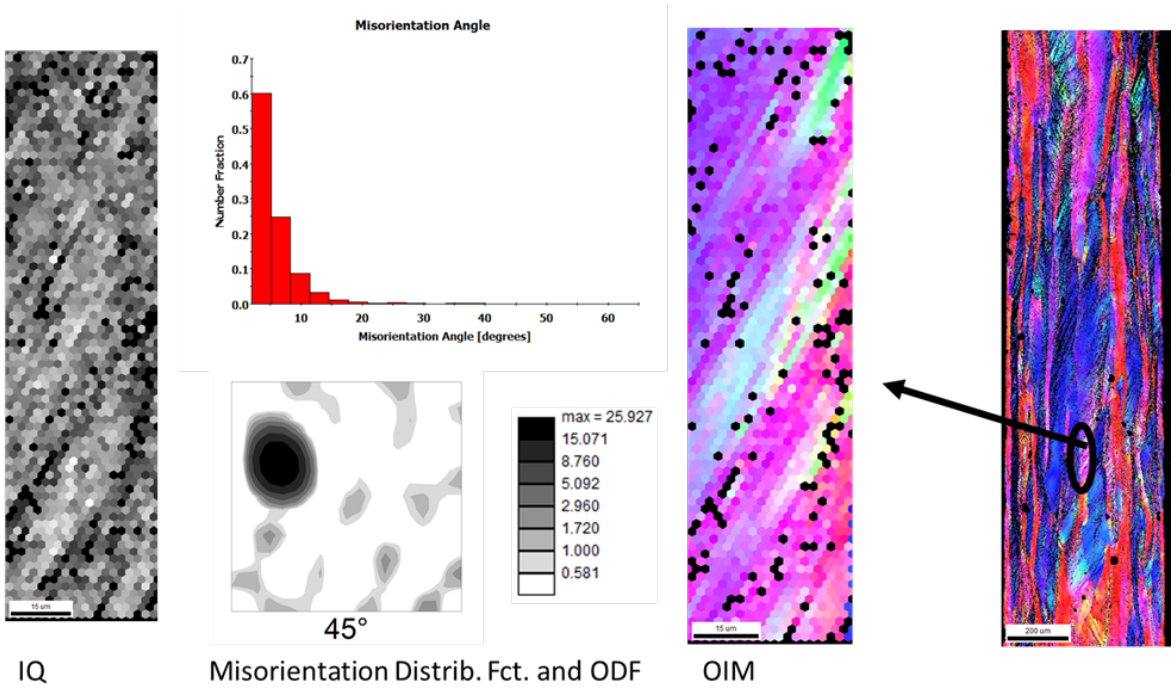

Fig. 3: Image quality plus the rotation angle map (misorientation), ODF OIM and distribution function for the misorientation for a selected area of sample 7 after cold deformation

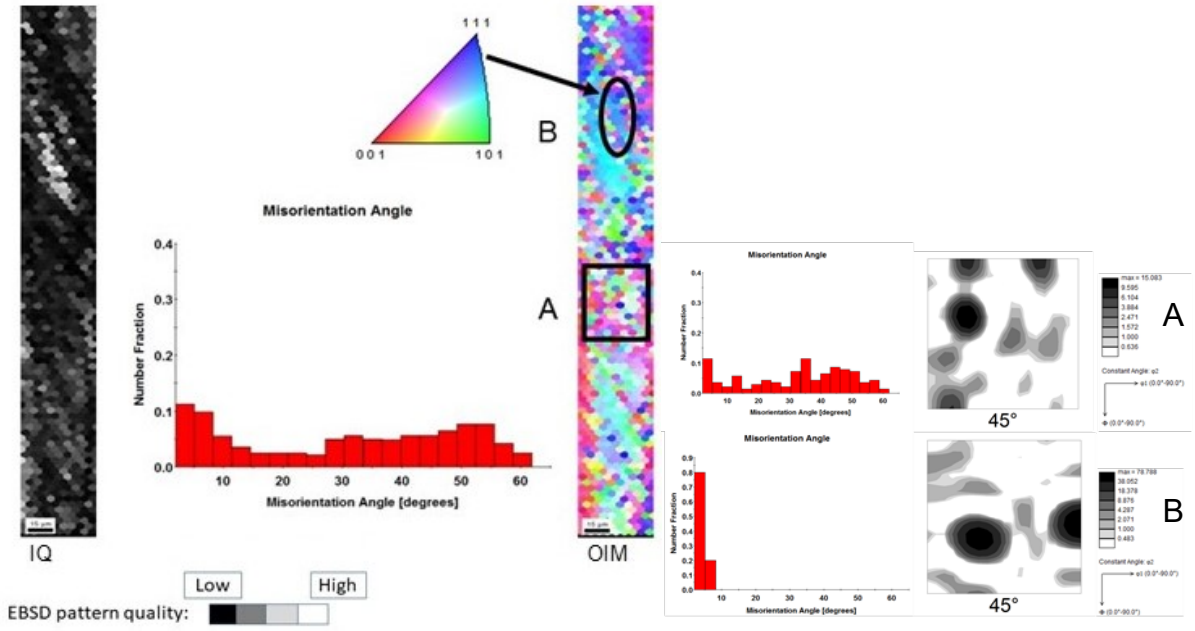

Fig. 4: Image quality plus the rotation angle map (misorientation), ODF OIM and distribution function for the misorientation for a selected area of sample 2 after cold deformation

2.2 Evolution of Microstructure and Texture after Annealing at Low Temperatures

The softening process at annealing at low temperatures comprises recovery and recrystallization. Recovery is characterized by cancellation and rearrangement of dislocations, which leads to the formation of sub grain structures with low angle boundaries and recrystallization by formation and subsequent motion of new high angle boundaries. [8, 9].
In the following we will analyse the recrystallization by regarding the results for annealing at different temperatures from 700°C to 800°C. The heating rate and the cooling rate were chosen like for a continous annealing. Figure 5 gives the image quality map plus rotation angle map (IQ plus misorientation) and the OIM after annealing at 700°C and 760°C for 20s. Red lines indicate small angle distribution (2°to 15°) and black lines large angles (>15°). After annealing at 700°C for 20s there exist bands with cube fiber texture in the middle of the sample like after cold rolling. Even after annealing at 760°C for 20 s one observes large elongated grains. Figure 6 presents the observed overall figure of the sample 2 for the texture (ODF) at annealing at 700°C and 760 °C with different annealing time compared to those after cold rolling.The intensity of the α – fibre disappears and of the γ – fibre increses with increasing the annealing temperature. An increase of the α^* - fibre and cube – fibre texture with increasing annealing temperature and annealing time is obtained. Even a small Goss texture intensity is found. The obtained figure indicates the role of the kinetic of the recystallization pocess on the texture formation.
Regarding Figure 1, 5 and 6, it seems that for sample 2 during the low temperature annealing after cold rolling the recrystallization is going on in the bands with γ – texture and a fragmentation appear in the bands with cube fibre texture. Finally, at 760°C complete recrystallization is observed. It should be mentioned that the resulting microstructure and texture at recrystallization depends on the different deformation structure after cold rolling, which depend again on the microstructure and texture of the hot band.
The mechanism of recrystallization comprises the process of nucleation and growth of the recrystallized nuclei in the deformed matrix.Thereby the stored deformation energy is the driving force. Assuming homogeneous in –plane compression strain the Taylor factor may be used to characterize the stored deformation energy (dislocation density) depending on the crystallographic orientation. This factor may be also used to describe the energetic situation between neighbouring grains in the case of nonuniform straining (strain partitioning, strain localization [10]). One distinguish on one hand at recrystallization subgrain growth in regions with high deformation energy (high stored energy mechanism [11]) and on the other hand subgrain growth of low energy crystallites in high energy stored crytallites (SIBM: bulging of a low energy region), see [10, 11]. This scenario one has to keep in mind regarding the recrystallization of our cold rolled material with such a complex heterogeneous deformation structure.

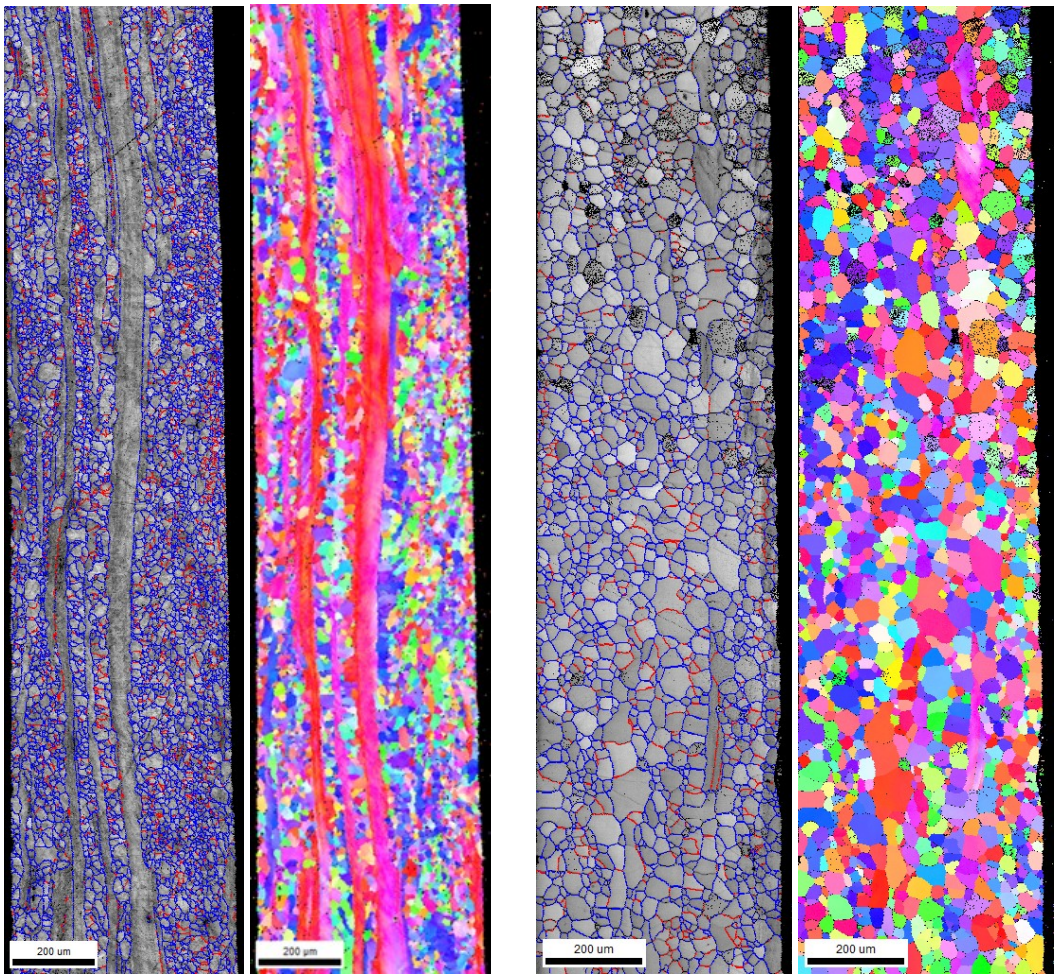

IQ_Mis OIM IQ_Mis OIM

Fig. 5: Image quality plus the rotation angle map (misorientation) and OIM of sample 2 after annealing at 700°C (left) and 760°C (right) for 20s

To see how the recrystallization process (formation of nuclei and growth of nuclei; formation of grain structure) is going on in detail across the thickness we analyzed for the sample 2 different areas across the thickness at annealing at 760°C with annealing time t_a= 0 and 20s. Figure7 gives the OIM of sample 2 after annealing at 760°C for 0 s across the thickness. Figure 8 presents IQ plus rotation angle maps and ODF for different areas across the thickness for sample 2, see Figure 7, after annealing at 760°C with annealing time t_a= 0**.** Figure 9 shows IQ and ODF in different areas, as indicated, for sample 2 after annealing at someone higher temperature of 760°C for 20 s.

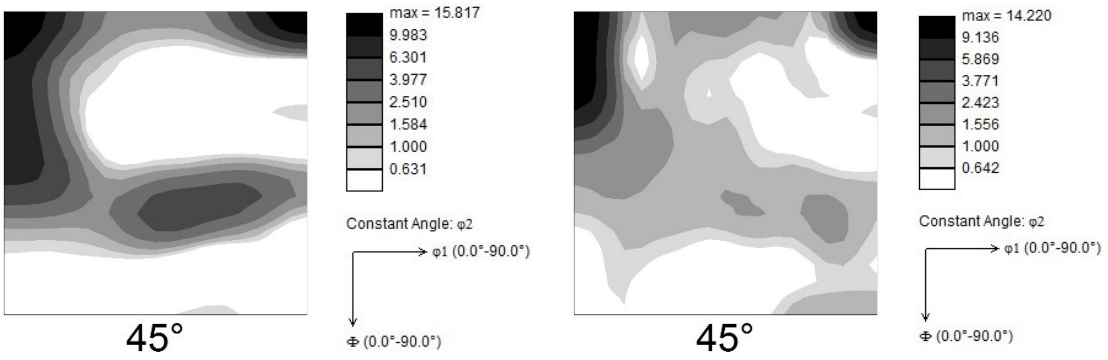

Sample 2 after CR Sample 2: 700°C / 20 s

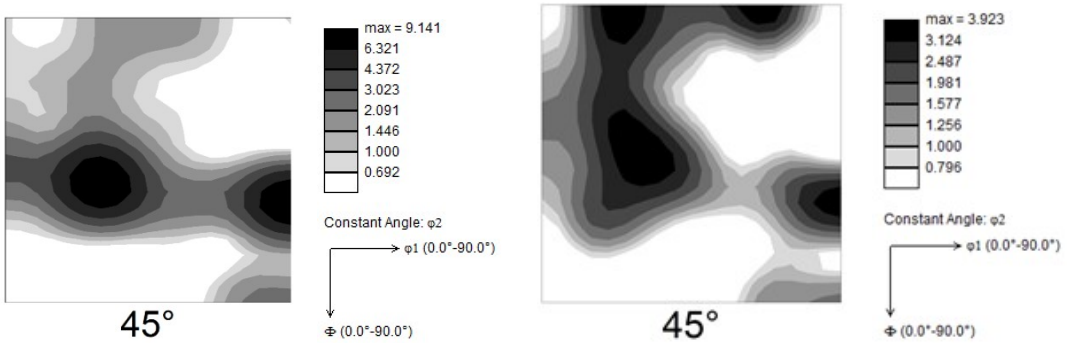

Sample 2 760°C/0s Sample 2 760°C/20s

Fig. 6: ODF for sample 2 after cold rolling and annealing at 700°C as well as 760°C for different annealing time

We observe in both cases a rather inhomogeneous figure of the microstructure and texture for annealing at 760°C with annealing time ta = 0 as well as ta = 20s. Characteristic feature for the texture formation is a decrease of α – fibre texture as well as a decrease of the γ – fibre, at least at larger annealing time. With respect to the preferable magnetic texture components for NGO (cube texture, cube fibre texture, α^* - fibre texture) the intensity is higher in areas with lower grain size. The distribution of misorientation for the region with small grains has a much lower intensity of small angles and a high intensity of large angles between 30 and 40 degree, see Figure 9. The area with larger grains may result from even larger elongated grains by recovery related to higher intensity of small angle boundaries. At 760°C we have already a complete recrystallized microstructure. It appears that the figure for the texture changes with the growth of nuclei and formation of grain structure by grain growth. Experimentally, in-situ EBSD investigations may help to clarify the role of the bands with γ- texture or cube fibre texture as well as of the zones with shear banding after the cold rolling on this process.

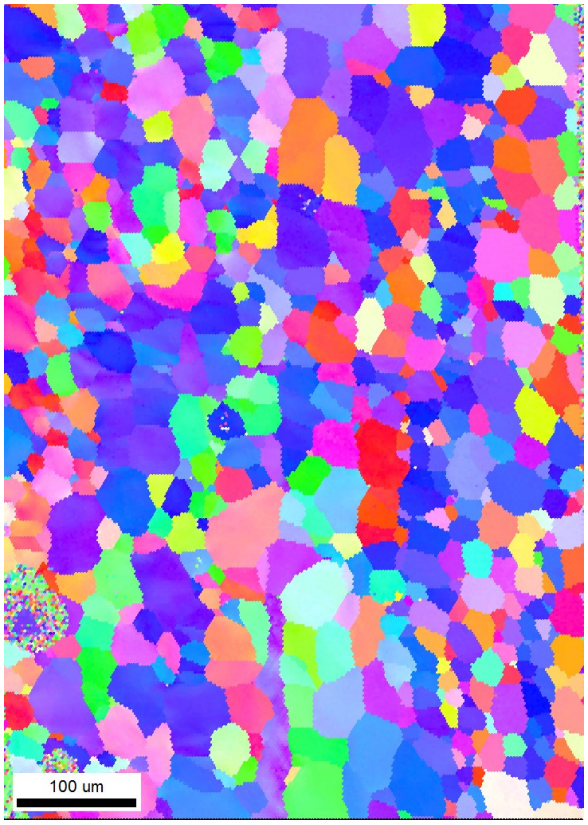

Fig. 7: OIM of sample 2 after annealing at 760°C for 0 s

The obtained figures for the texture cannot be explained by subgrain growth into regions with high deformation energy due to high values of the Taylor factor by uniform in-plane strain. The deformation structure in the regarded case is much more complex, as described. We may regard that shear strain exist beside uniform in-plane strain. The Taylor factor in the case of a superposition of in-plane strain and shear strain results in a different figure for hard orientation (large Taylor factor) and soft orientations (low Taylor factor), see Figure 10 and [3. 12]. Larger intensity of shear strain to plane strain compression results finally in a shift of “hard” and “soft” directions, see Figure 10. At increasing shear stress we have cube, cube fibre texture and α^* - texture as “hard directions“. These points to the importance of shear bending across the sample thickness to get a high intensity of magnetically relevant texture components at recrystallization. We may now assume that we may have recrystallization by nucleation or by SIBM. Recrystallization comprises nucleation and growth of nuclei in the deformed matrix, which is characterized by subgrain growth in regions with high deformation energy (high stored energy mechanism).

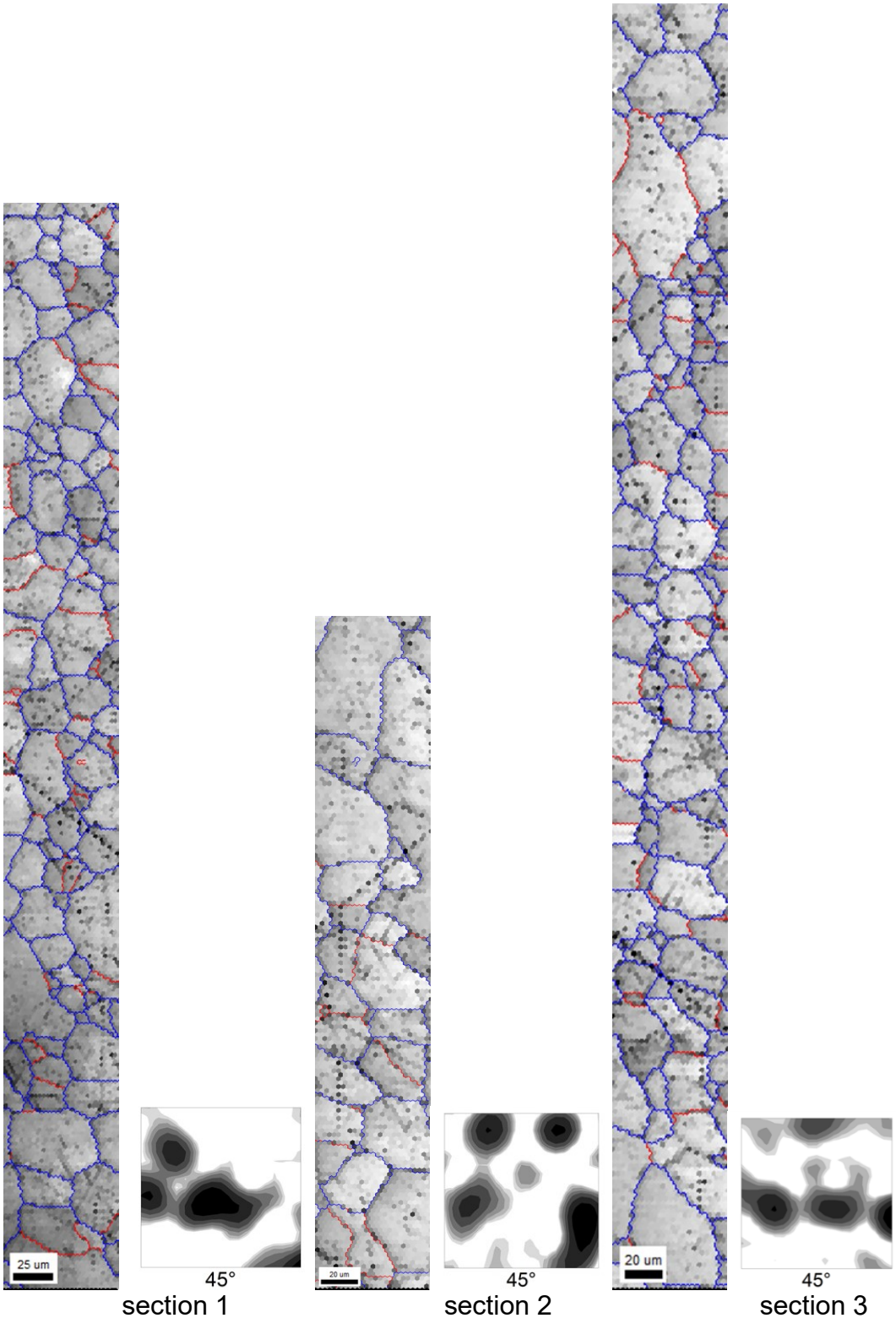

Fig. 8: IQ plus rotation angle maps and ODF for different areas across the thickness for sample 2 after annealing at 760°C with annealing time t_a= 0

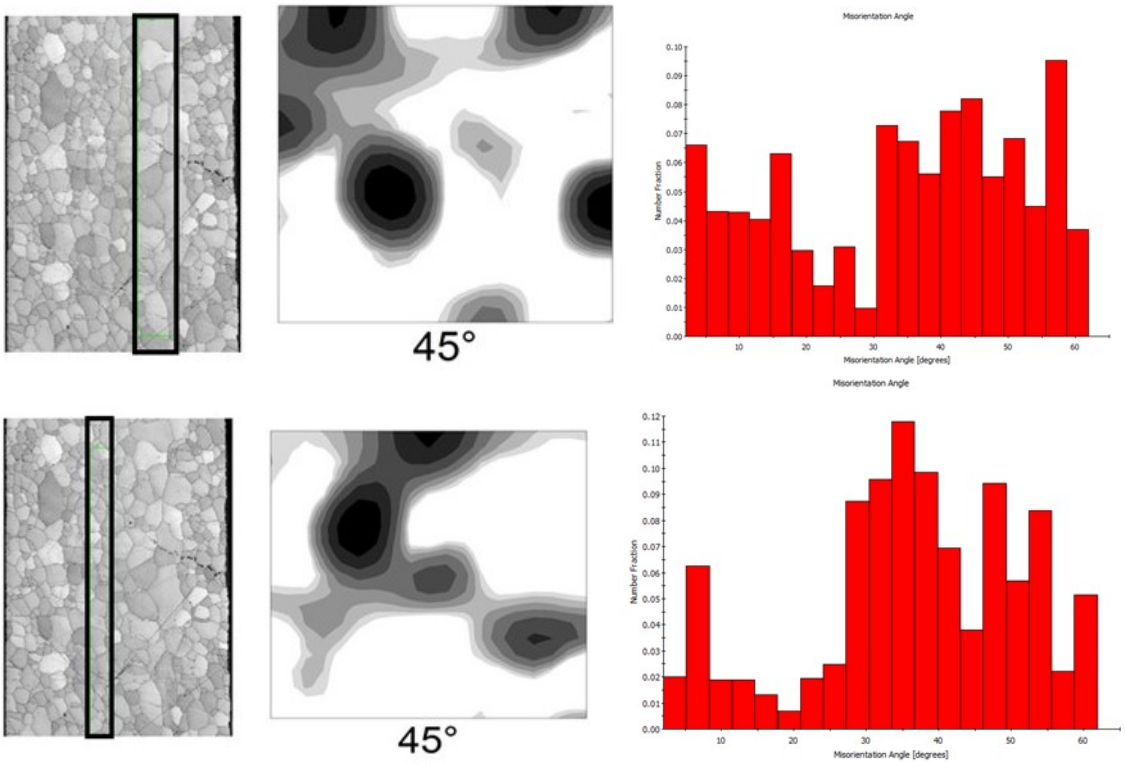

Fig. 9: IQ and ODF in different areas, as indicated, for sample 2 after annealing at 760°C for 20 s

This results in growth in the orientations associated with a high Taylor factor (only uniform in-plane strain or superposition of uniform in-plane strain and shear strain). SIBM describes the process of subgrain growth of low energy crystallites in high energy stored crystallites (SIBM: bulging of a low energy region). A process, where grains with the lower stored energy grow up in the neighbouring crystal [8] in the case of already existing grains. The changes of the intensities of the magnetically relevant magnetic texture components at low temperature annealing of sample 2, see Figure 6,8 and 9, may be explained in this way by a superposition of nucleation and SIBM. For areas with K=0 (only uniform in-plane deformation) we may have rotated cube by SIBM and cube texture by nucleation. For areas with K > 1 α^* - texture appears by nucleation. It should be remarked that we may have beside SIBM already secondary recrystallization, especially in regions, where only large angles boundary exist. It should be also mentioned, that the occurrence of grain growth by SIBM in our case is similar to the ongoing process at the beginning of annealing for semifinished FeSi steels (CRLS), where grains exist at the beginning of thermal annealing after temper rolling.

2.3 Evolution of Microstructure and Texture after Annealing at High Temperatures

We will regard sample 1 and 2. While at annealing of sample 1 at 800°C we have still a remarkable intensity of small angle boundaries in the middle of the sample 1. Whereas sample 2 exhibits only a low intensity of small angle boundaries, see Figure 11. At annealing above 800°C there are practically a very low intensity of small angle and grain structure exist across the thickness (recrystallized microstructure).The OIM and ODF after annealing at 800°C, 900°C and 1050 °C are given in Figure 12 and 13

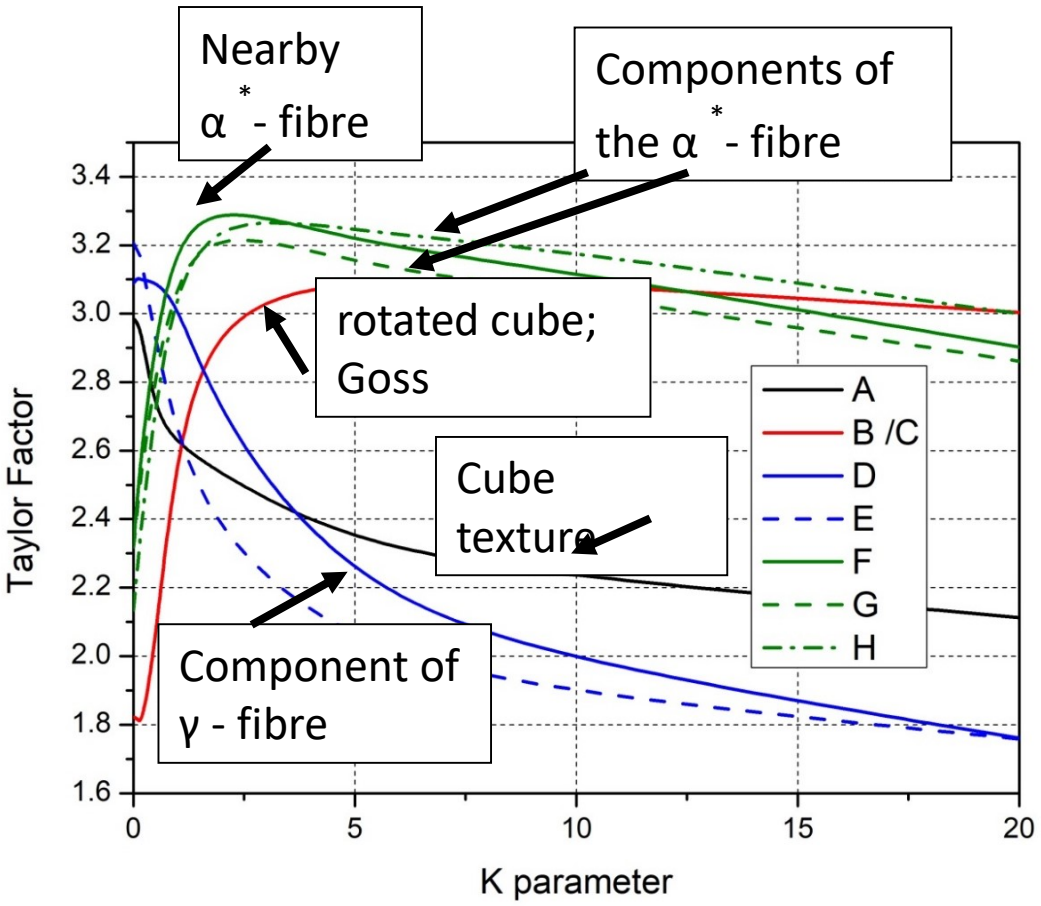

Fig. 10:Taylor factor as function of the K (K characterize the shear stress; K = 0 no shear stress)

A – {100}<001> cube texture, B –100}<110> rotated cube texture, C – {110}<001> Goss texture; D - component {111}<112> of the γ – fibre; E – component {111}<121>, F – {113}<251>; G - component {113}<136> of the α^* - fibre ; H – component {411}<148> of the α^* - fibre, F = {113}<251>, G = {113}<136>, H = {411}<148>

As can be seen, the grain size increases with increasing annealing temperature in an inhomogeneous way. The influence using cold rolled material from different fabricated hot band on the evolution of texture is clearly seen in Figure 12 and 13. At annealing at higher temperatures the ongoing processes start also from the microstructure of the cold rolled state. It can be assumed that first recovery followed by recrystallization appear. The recrystallization involves nucleation characterized by appearance of nuclei and growth of the recrystallized nuclei in the deformed matrix. Depending on the nature of the strain also SIBM occur. In the fully recystallized microstructure finally one may have an increase of the grain size by secondary recrystallization (inhomogeneous increase of the size of the grains [8]).

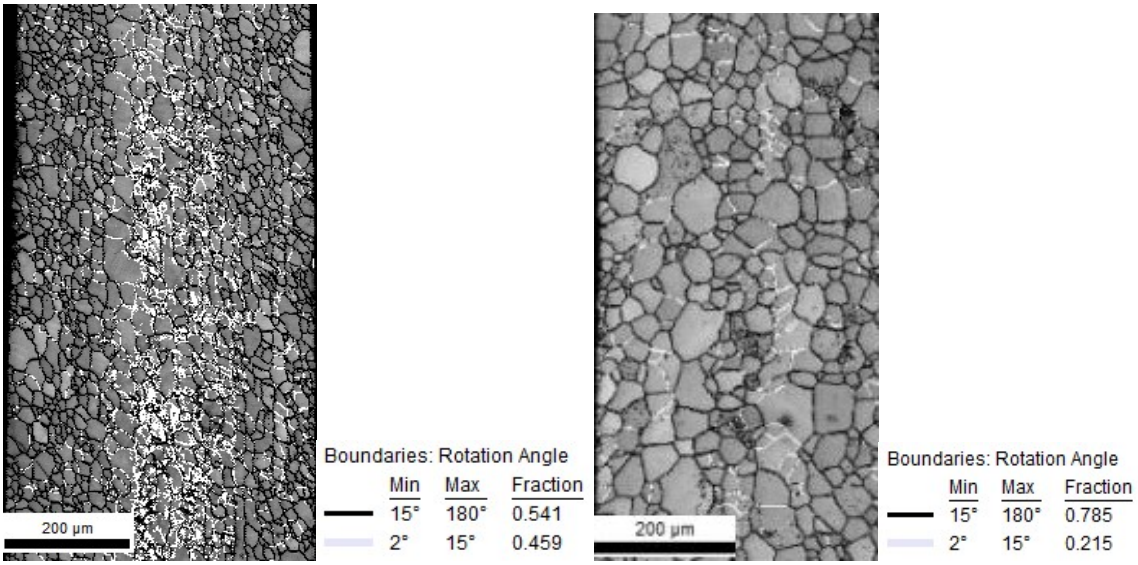

Sample 1: 800°C/20s Sample 2: 800°C/20

Fig. 11: IQ plus rotation angle maps for sample 1 and 2 after annealing at 800°C for 20 s

The progress of these different processes is affected by the annealing conditions: heating rate, maximum annealing temperature and holding time at this temperature. Due to the rather inhomogeneous and complex deformation structure in the cold rolled state across the thickness these processes may appear simultaneously. Even SIBM may arise adjacent to secondary recrystallization.This figure for the ongoing process sequence at annealing at higher annealing temperature is supported by the obtained results for the evolution of the microstructure at annealing at 750°C for different annealing times. Figure 14 shows the OIM and ODF for sample 1 for annealing at 750°C at different annealing time. The results for sample 2 you may find in [13].

Regarding the secondary recrystallization, the driving force of abnormal grain growth (secondary recrystallization) is the reduction of the total internal surfaces (Grain Boundaries -GBs) by elimination of GBs with higher energy (energy minimization) [8, 14]. One has to regard the grain boundary energies as well as the grain boundary mobility. GB energy is not homogeneous and may be different for a regarded grain with respect to the neighbouring grains. The grain boundary character is described by the misorientation with respect to the neighbouring grains. The grain boundary energy varies with the crystallographic nature of the boundary. At present, there is no general model to calculate the grain boundary energy for different nature of the boundary [14]. There are also no data by measurements for the regarded ferritic FeSi. There exists no data on the energy ranking of the grain boundary energy for different misorientation of the neighbours. With respect to the mobility one may regard the relation between the obtained figure for the texture and the occurence of CSL-boundaries. CSL boundaries are preferred at grain growth, especially in the range of θ between 20 and 40 degree [15]. In addition, one has to consider the precipitation structure [8].

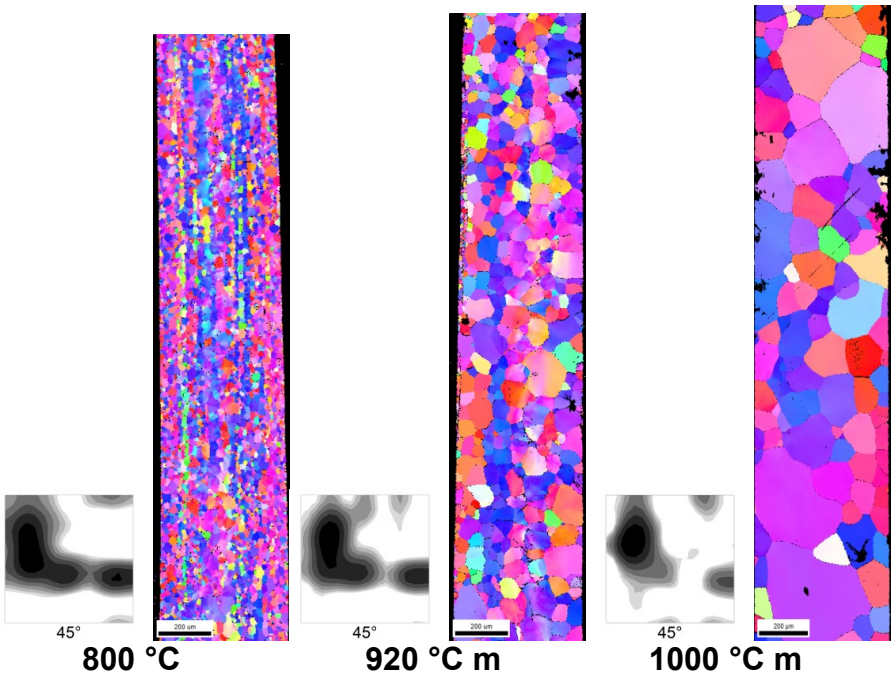

Fig. 12: ODF (averaged values across different EBSD measurements across the length) and the OIM for a selected length at annealing at high temperatures for sample 1

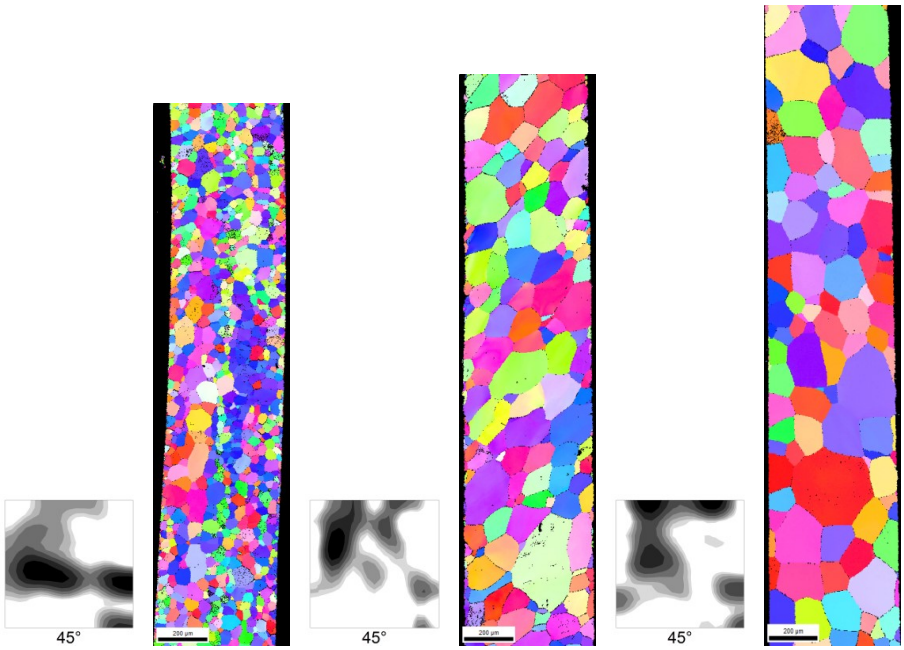

Fig. 13: ODF (averaged values across different EBSD measurements across the length) and the OIM for a selected length at annealing at high temperatures for sample 2

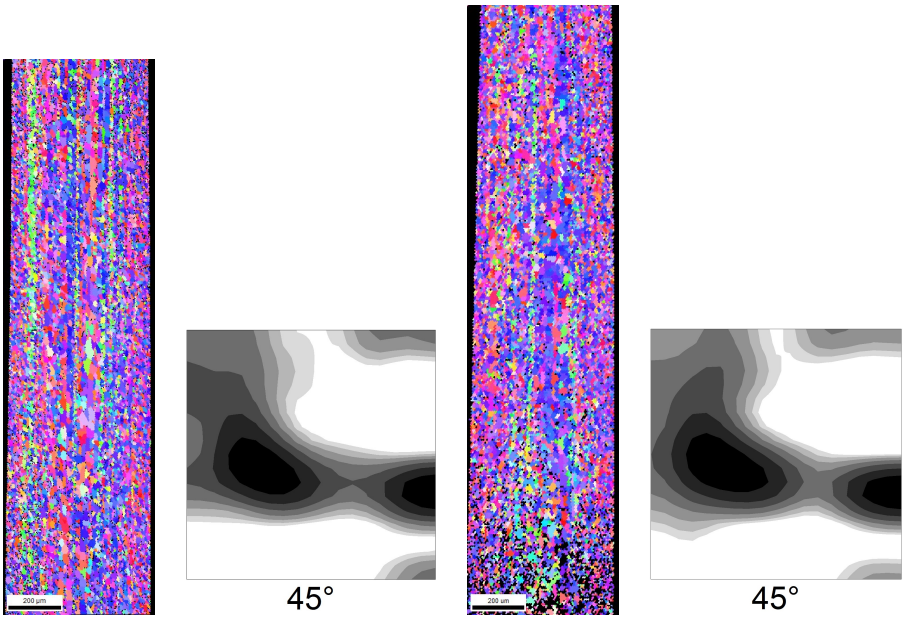

Fig. 14: OIM and ODF for sample 1 for annealing at 750°C and an annealing time of 1 min (left) and 5 mim (right)

3 Summary and Conclusions

The electrical steels demand beside a high intensity of preferable magnetic texture components for improved magnetization behaviour large values of the grain size to reach the desired low values of the specific magnetic losses. The demand for large grain size needs an annealing at higher temperatures to get beside a recrystallization also a grain enlargement by normal or abnormal grain growth (secondary recrystallization).

The large deformation rate at cold rolling results in a rather complex spatial inhomogeneous figure for the deformation. In addition, the microstructure and texture of the hot band has an important influence on the heterogenous deformation structure after the cold rolling. The nature of the localized strain in the cold rolled state is different. This results finally in a different character of the recrystallization process at final annealing across the thickness. This affect the resulting figure for the texture. Preferable magnetic texture components are obtained in the case that shear bending acoss the thickness is present.

The evolution of the microstruture and texture at final annealing cannot be desribed only by recrystallization. Grain enlargement by normal or abnormal grain growth (secondary recrystallization) has to be regarded too, at annealing at higher temperatures.

Due to the complexity of the processes, which depend also on the annealing conditions, a prediction of the resulting figure for micostructure and texture at final annealing of the ferritic FeSi steels can be hardly done. A model, which can describe the ongoing processes according to the annealing conditions does not exist.

The understanding of all these different processes on the evolution of microstructure texture demands further work. This comprises a clear identification between the various mechanism at recrystallization as well as between SIBM and secondary recrystallization. Models for the grain growth for these ferritic FeSi steels at secondary recystallization are also missing. A crucial point thereby is to describe the effect of the texture of the neighbouring grains on the growth of a regarded grain.

4 References

[1] A. Franke, J. Schneider, B. Bacroix, and R. Kawalla, Proc. of the 8th International Conference on Magnetism and Metallurgy, Dresden, June 2018, publ. By Universitätsverlag TUBAF, ISBN 978-3-86012-579-3

[2] A.Franke, J. Schneider, B. Bacroix B., and R. Kawalla,, Invited Paper at the Conference Re&GG2019, *August 2019, Ghent Belgium*

[3] A. Franke,*, J. Schneider, B. Bacroix, and R. Kawalla, Journal of Material Science and Technology Research, 2018, 5, 28-38

[4] A. Franke, J. Schneider, B. Bacroix and R. Kawalla, Journal of Material Science and Technology Research, 2019, 6, 89-109).

[5] Hai-Tao LIU , J. Schneider , A. Stöcker , A. Franke , Fei GAO , Hong-Yu SONG, Zhen-Yu LIU , R. Kawalla and Guo-Dong Wang, steel research int. 87 (2016), p.589;
[6] J. Schneider, A. Franke, A. Stöcker, H.-T. Liu, G.-D., Wang, R. Kawalla, IEEE Trans. on Magnetics (2016)
[7] Mehdi Sanjari , Youliang He,Erik J. Hilinski, Steve Yue, and Leo A. I. Kestens, Journal of Materials Science, published online: 28 November 2016).
[8] G. Gottstein, Physikalische Grundlagen der Materialkunde, Springer Berlin Heidelberg 2007
[9] D. Raabe, Physical Metallurgy, 5th Edition, Elsevier (2014), p.2291 – 2397
[10] B. Hutchinson, Material Science Forum Vols 558 – 559 (2007) 13
[11] L. Kestens, L. Bracke, K. Verbeken and R.H. Petrov; Paper at Conference Plasticity 2009, Saint-Thomas (2009) 3 – 8 January
[12] B. Bacroix, J. Schneider and A. Franke, IOP Conf. Series: Journal of Physics: Conf. Series 1270 (2019) 012007
IOP Publishing doi:10.1088/1742-6596/1270/1/012007
[13] J. Schneider, A. Stöcker, A. Franke, and R. Kawalla, AIP Advances 8, 047606 (2018); doi: 10.1063/1.4993526
[14] A. Rollet, Carnegie. Mellon. MRSEC, 27-750. Texture, Microstructure & Anisotropy
[15] Y. Hayakawa and J. A. Szpunar, Acta Mater. (1997) Vol. 45, p.4713